Contact-line mechanics for pattern control†‡

Guillaume Miquelard-Garnier,§ Andrew B. Croll,§ Chelsea S. Davis and Alfred J. Crosby*

Received 26th March 2010, Accepted 12th July 2010
DOI: 10.1039/c0sm00165a

Wrinkled surfaces are ubiquitous in Nature and can be used in a large range of applications such as improved adhesives, microfluidic patterns, or as metrology instruments. Despite wide-ranging applications, existing methods do not permit local pattern control since all existing methods impose extensive compressive strains. In this article, we describe a new process that exploits the local deformation of a soft substrate as it stretches to form an adhesive interface with a thin polymer film. The wrinkle pattern is effectively a measurement of the strain-field created during the adhesion process, which shows a strong dependence on the speed of attachment. We develop simple scaling arguments to describe this velocity dependence and a critical velocity above which wrinkles do not form. Notably, our approach allows us to define the surface pattern "wrinkle-by-wrinkle", thus permitting the creation of single wrinkles. Intricate patterns on laterally extensive length scales can also be produced by exploiting the shape of the contact line between the film and the substrate. This level of control—the placement of single features of prescribed trajectory—which is not present in any other method of thin film wrinkling, is absolutely necessary for any realistic, scalable application.

Introduction

Thin films are commonly laid onto solid substrates in the fabrication of multilayer devices, layer-by-layer composites, and even wound closures. In these processes, the three phase contact line between the thin film, the solid substrate, and the gas or liquid phase surrounding the two, unique in its one dimensionality and locality, gently sweeps across the sample creating a two dimensional interface. Classically, interfacial energies at the three phase contact line between two solids balance with the elastic restoring forces as a solid–solid interface develops. In this article, we show how a contact line can dominate a system's behavior when a thin, solid capping layer adheres to a soft substrate, ultimately providing a unique tool for creating localized patterns across laterally extensive lengths. In particular, the narrow deformation of the substrate caused by the contact line is sufficient to buckle the thin plate and locally wrinkle the system.

When a sufficient compressive strain is applied to a bilayer consisting of a thin, stiff film bound to a softer and thicker substrate, a mechanical instability takes place.[1] The instability is due to the balance between the energetic cost of bending the film and of stretching the substrate which results in a sinusoidal surface deformation known as wrinkling.[2–10] Because of their cost-effectiveness and simplicity, wrinkled surfaces can be used for a large range of applications, for example optical surfaces,[11,12] enhanced adhesives,[13,14] soft-lithographic structures,[15] microfluidic devices[16,17] or cell culture surfaces.[18] Several methods have been developed to control the applied strain (thermal expansion mismatch,[3] traction,[5,7,10] or solvent swelling of the substrate[8,12]); however, they are all inherently non-local processes and therefore difficult to use in the fabrication of complex devices.

In this experiment, an elastomeric substrate is immersed in a water bath and brought into contact with a thin floating polymeric film. As the substrate is pulled out of (or pushed into) the water, the contact line pulls on the substrate, deforming it out of its originally flat state.[19,20] The locally stretched substrate adheres to the inextensible film at the contact line, and as the contact line passes, the stretched region of the substrate relaxes, thus imposing a compressive stress in the film. If the stress is great enough, the film wrinkles (Fig. 1 and Experimental section for more details). We note that this is the first achievement of a locally controlled method of applying strain to a bilayer, with clear implications for the industrial realization of wrinkled devices and coatings.

Results and discussion

The wavelength of the wrinkles, λ, is intermediate between the length scale which is natural for a bent plate ($\sim$the plate size) and the nanoscopic length scale of the elastomer ($\sim G/E_S$ where G is the interfacial adhesion energy and E_S is the modulus of the substrate). Under the assumption of small strain, the wavelength is given by:[2]

$$\lambda = 2\pi t\left(\frac{\bar{E}_f}{3\bar{E}_s}\right)^{1/3}, \quad (1)$$

where t is the thickness of the capping film, $\bar{E} = E/(1 - \nu^2)$ is the plane-strain modulus with Young's modulus given by E, and Poisson's ratio ν. The subscripts f and s refer to the capping film and substrate, respectively. This equation is valid for both uniaxial and biaxial compressions and has been used extensively.[2–10] Under the same framework, the amplitude of the wrinkles, A, is given by:[2]

Polymer Science & Engineering Department, University of Massachusetts, 120 Governors Drive, Amherst, 01002, MA, USA. E-mail: crosby@mail.pse.umass.edu

† This paper is part of a *Soft Matter* themed issue on The Physics of Buckling. Guest editor: Alfred Crosby.

‡ Electronic supplementary information (ESI) available: Velocity dependence of the motion of a contact line during adhesive contact between two bodies. See DOI: 10.1039/c0sm00165a

§ These authors have contributed equally to this work.

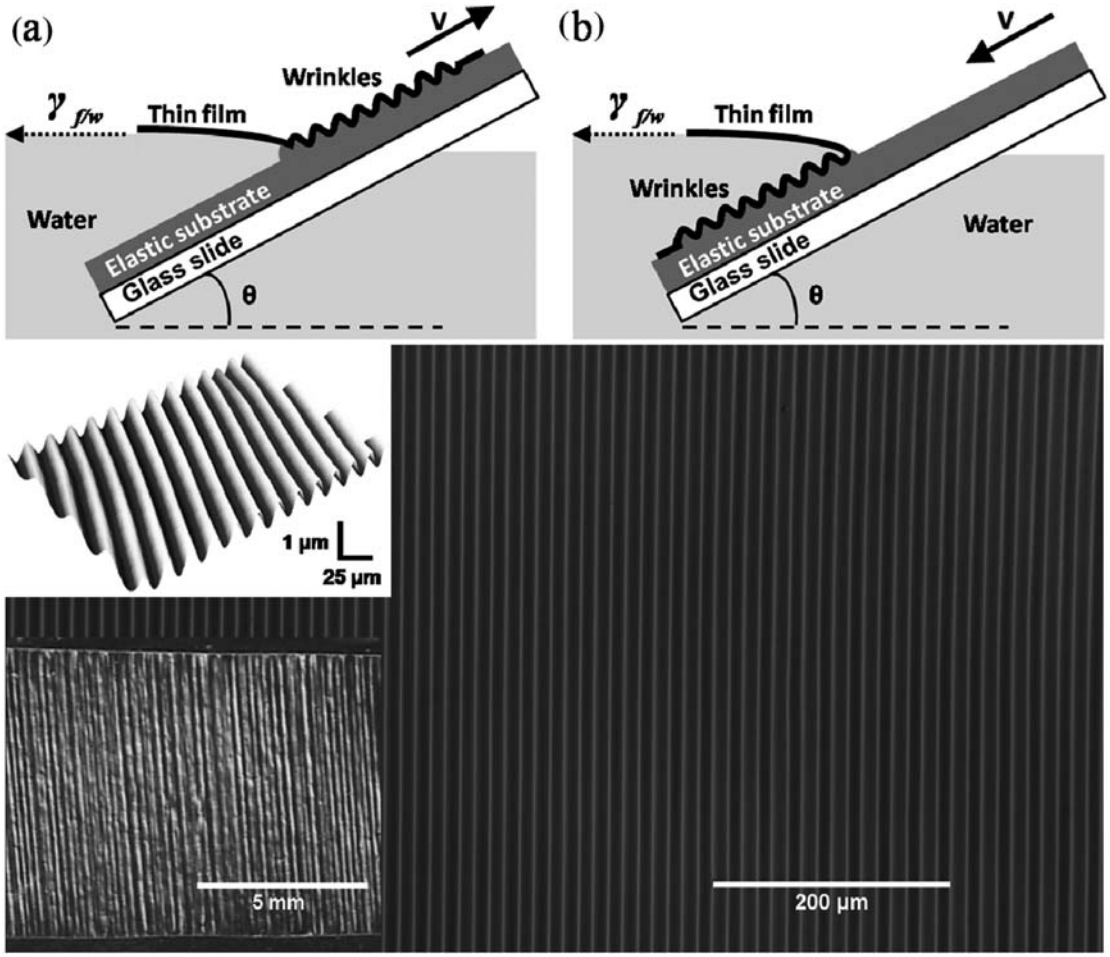

Fig. 1 Basic experimental schematic and results. Top: the experimental set-up. (a) The PDMS substrate is pulled out of the water at chosen speed and angle and wrinkles form. (b) Wrinkles are also obtained when the experiment is reversed, *e.g.* when the substrate is pushed in the liquid: in that case the three point contact line is air–film–substrate and not water–film–substrate. Bottom: optical images of the wrinkles obtained: optical profilometry picture (top inset), wrinkles over the whole PS sheet (bottom inset) and zoomed using a 10× objective.

$$A = t\left(\frac{\varepsilon}{\varepsilon_c} - 1\right)^{1/2}, \quad (2)$$

where ε is the applied compressive strain and ε_c the critical buckling strain, the maximum strain that can be applied to a plate before it wrinkles. For uniaxial strain:

$$\varepsilon_c = 1/4(3\bar{E}_s/\bar{E}_f)^{2/3}. \quad (3)$$

Eqn (1) is markedly independent of strain and is ideal for comparison to our experiments where adhesion imparts an unknown strain. Thus, at a given speed of withdrawal (0.1 mm s^{-1}) and angle (45°) with respect to the water surface, we measured the wavelength on samples with different types of elastomeric substrates (chemical structure and moduli) and polystyrene films with different film thicknesses and molecular weights (Fig. 2a). Assuming typical values for Poisson's ratio $\nu_s = 0.5$ for the elastomer, $\nu_f = 0.33$[21] for the PS films, the modulus of the PS films $E_f = 3.5$ GPa[5] and using independently measured values of E_s (see Experimental section), eqn (1) is seen to fall on the data with *no* fitting parameters (Fig. 2a). Moreover, both changes in angle and speed do not have significant impact on the wavelength of the wrinkles. We are therefore confident that this technique in no way alters the underlying physics; it simply creates a local compressive strain.

Notably, the amplitude of the wrinkles is observed to be a monotonically decreasing function of substrate velocity. We also observe that no wrinkles form (amplitude falls to zero) in the "pull out" geometry when the substrate speed exceeds a critical value close to 1 mm s^{-1}, whereas the "push in" scenario always gives rise to wrinkles up to the limiting speed of our motorized stage (Fig. 2b). Because the main difference between the two experiments is the fluid between the film and substrate, the hydrodynamics of the coating process must play some role in the wrinkling mechanism, which we address below.

According to eqn (2), the variation in amplitude must be related to a change in the applied strain as film thickness and moduli (*e.g.* critical strain) are fixed in a given sample. Therefore, we plot strain calculated directly from $\varepsilon = (\pi t/\lambda)^2(A^2/t^2 + 1)$, as a function of velocity in Fig. 2c. The amount of strain that is applied to the sample is due to the difference in contour length of the deformed surface compared to the inextensible film. The true surface deformation can be approximated by assuming an adhesive force is applied to a line on the substrate surface, *i.e.* an

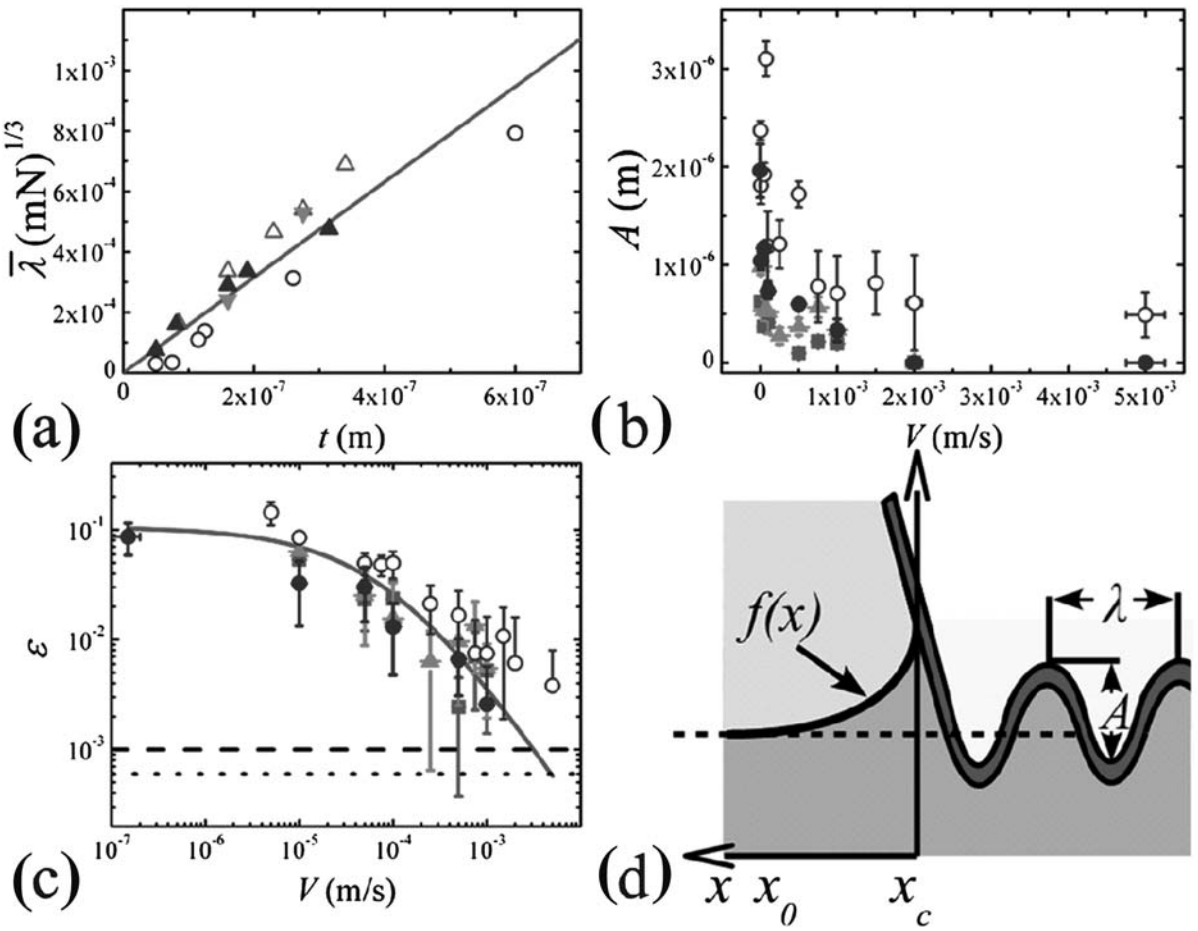

Fig. 2 Detailed measurements of the wrinkles created by contact line motion. (a) Scaled wrinkle wavelength, defined as $\bar{\lambda} = \lambda \frac{(3\bar{E}_S)^{\frac{1}{3}}}{2\pi}$, of polystyrene on several different substrates as a function of film thickness (substrates: 40 : 1 PDMS—filled upward pointing triangles, 30 : 1—open upward pointing triangles, 20 : 1—filled downward pointing triangles, triblock gel—open circles). Solid line is the predicted fit using eqn (1). (b) Amplitude of wrinkles as a function of stage velocity (squares—30 : 1 PDMS with 82 nm PS film, triangles—40 : 1 PDMS with 82 nm PS film, closed circles—40 : 1 PDMS with 160 nm PS film, open circles—dipping into fluid 40 : 1 PDMS with 225 nm PS film). (c) Strain as a function of stage velocity for the data shown in (b). Solid curve denotes a fit to eqn (3), with $(P/G_0)^2 = 0.106$ m^2, $n = 0.642$ and $V^* = 9.73 \times 10^{-5}$ m s^{-1}. The dashed line denotes the critical strain in 30 : 1 PDMS samples and the dotted line denotes the critical strain in 40 : 1 PDMS. While the 30 : 1 samples may be near the critical strain at $V \approx 1$ mm s^{-1}, the 40 : 1 samples remain significantly above the cut off indicating that another mechanism is causing the amplitude to drop to zero. The sample created by dipping into the water (rather than pulling out) shows no cut-off at $V \approx 1$ mm s^{-1} suggesting the hydrodynamics of the coating process plays a role. (d) Schematic showing the details of the contact line as a thin film is attached to a soft substrate (dark grey). The fluid between the substrate and the film is in light grey, the dashed line represents the undeformed surface of the substrate before attachment.

inverted 'knife edge' problem.[22] The elastomer surface as a function of distance from the contact point is given by $f(x) \approx (P/\bar{E})\ln(x_0/x)$ where P is the normal component of the tension in the film, and x_0 is the distance at which the perturbation becomes negligible (Fig. 2d). The differential strain at the contact line is then evaluated by comparing the difference between an undeformed element and an element along $f(x)$ (*i.e.* $\varepsilon \approx (\mathrm{d}s - \mathrm{d}x)/\mathrm{d}x \approx \sqrt{1 + (f')^2} - 1$ where f' is the derivative of $f(x)$). The differential strain is calculated at x_c, the smallest length scale available before the breakdown of the continuum approximation (in an elastomer $x_c \approx G/E$). Ultimately this calculation yields the scaling relation $\varepsilon \approx P^2/G^2$. In this particular experiment, the applied force P is due to the unbalanced surface tension at the floating free edge of the polymer film (*i.e.* $\sim\gamma_{flw}$). Such deformations of soft elastomers due to surface tension forces have already been observed experimentally[20,23] and it can be easily verified in our case by the addition of surfactant to the water surface (samples fail to wrinkle). This force will not strongly depend on the speed of the contact line (ignoring hydrodynamic losses). The relationship between applied strain and speed is mainly due to the strong velocity (V) dependence of G. For the polydimethylsiloxane [PDMS] elastomer used here it is known that $G(V) \approx G_0(1 + (V/V^*)^n)$, where n is close to 0.6 and V^* is related to the relaxation of the substrate (see ESI‡ or ref. 24). Therefore the applied strain scales as:

$$\varepsilon \approx \frac{P^2}{G_0^2(1 + (V/V^*)^n)^2} \tag{4}$$

The clear agreement between eqn (4) and the data (Fig. 2c) verifies the dominance of the elastomeric losses.

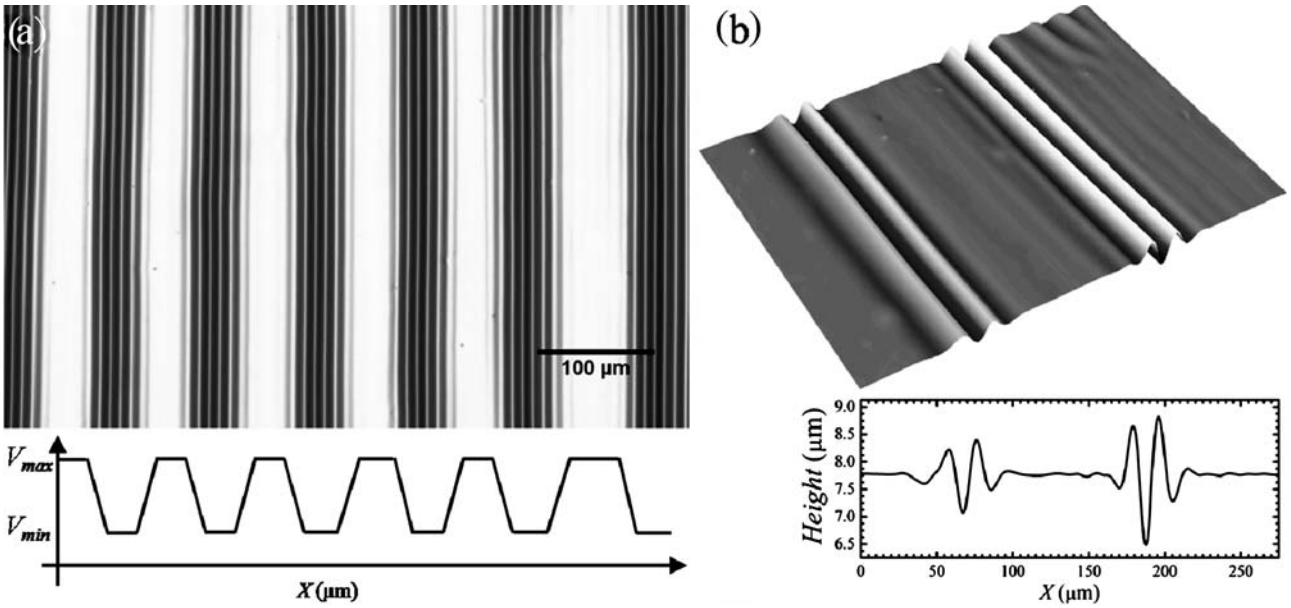

Fig. 3 Use of the critical speed to design localized patterning on thin films. (a) Series of regularly spaced aligned wrinkles by setting V_{max} above the critical value ($V_{min} = 0.01$ mm s^{-1} here). The brighter wrinkles have a smaller amplitude, due to the acceleration of the motor before reaching the experimental speed. Using the same technique with V_{max} below the critical speed, a continuous pattern with localized differences in amplitude can be obtained (data not shown). (b) Single features (ridges) were obtained using this technique. Note that the control of the amplitude is illustrated in the height profile below ($V_{min} = 0.1$ mm s^{-1} for the left ridge, $V_{min} = 0.01$ mm s^{-1} for the right ridge).

As already mentioned, the amplitude is also shown to drop to zero above a withdrawal speed of 1 mm s^{-1} in the "pulling out" experiment (Fig. 2b). One might expect that this is simply a result of ε falling below ε_c; however, Fig. 2c shows clearly that this is not the case. The coating of a substrate by withdrawal from a fluid bath is a classic example of capillarity and predicts a dramatic shift in behaviour of the contact line motion.[25–27] If the fluid wets the surface (*e.g.* when $S > 0$, where $S = \gamma_{sv} - \gamma_{sl} - \gamma_{lv}$ is the spreading parameter and the subscripts s, v, and l refer to the substrate, vapor phase, and liquid respectively) a coating will always be formed when the substrate is pulled from the bath as there is no energy gained by uncovering the substrate. In contrast, if the fluid does not completely wet the substrate ($S < 0$) the answer is found to depend on the velocity of the plate (V), with the fluid covering the substrate only above some critical speed (V_c).[25,26] If a non-viscous fluid coating forms between the polymer plate and the substrate the strain will not be "locked in" at the contact line and wrinkles will not form. Although the exact details of the hydrodynamic processes occurring at the contact line remain controversial,[25–27] the simplest scaling description[26] is sufficient to estimate the critical velocity: $V_c \approx \gamma_{lv}(1 - \cos\theta_e)^3/750\eta$, where $\cos\theta_e = \gamma_{sl} - \gamma_{sv}/\gamma_{lv}$, and η is viscosity.

Here $\gamma_{lv} \approx 0.03$ N m^{-1}, $1 - \cos\theta_e \approx 0.3$, and $\eta \approx 1 \times 10^{-3}$ m^2 s^{-1} which gives $V_c \approx 1$ mm s^{-1}, in agreement with our measurements. Importantly, this critical velocity can be manipulated by changing the properties of the fluid phase. For example if the geometry is reversed and the substrate is driven into the fluid bath, the fluid being expelled from between the plate and substrate is air and V_c increases dramatically (see Fig. 2b and c).

The control of the magnitude and direction of the strain using the motion of the triple line and the existence of a "critical speed" are unique properties that can be exploited to achieve pattern control that would be extremely difficult or impossible to attain using conventional techniques. We illustrate this versatility by developing a "stop and go" method as shown in Fig. 3a (*e.g.* coating the substrate at varying speeds above and below V_c in the "pulling out" case) which results in the creation of localized wrinkles (not folds).[28] Pushing this methodology allows the creation of isolated single ridges or "micro-channels" (Fig. 3b). Alternatively, stepping between two speeds below V_c allows the simple creation of a hierarchical surface.[10]

As the wrinkles form parallel to the contact line it is also possible to introduce a curvature in the pattern by using substrates displaying spatially controlled differences in hydrophobicity (Fig. 4a), which shifts the local curvature of the contact line. We are able to connect small features (channels) to bigger ones (*i.e.* interconnects) using a thin film presenting a gradient thickness perpendicular to the coating direction (Fig. 4b) as recently predicted theoritically.[29] Finally, circular wrinkle patterns can be achieved by introducing topographic curvature in the elastomeric substrate (Fig. 4c). Although film thickness and substrate curvature are well known to affect the resulting pattern, all these effects have to the best of our knowledge never been reported experimentally in the same system, despite the necessity of changing feature size from small to large (interconnects) and of direct control over wrinkle trajectory for the creation of realistic devices.[29–32]

Conclusion

In this paper we study the three phase contact line formed as a thin film is deposited on an elastomeric substrate. The result, an easily controlled wrinkle pattern, which obeys classical predictions of wavelength but shows a velocity dependent amplitude. The velocity dependence allows us to demonstrate how our experiment exploits adhesive processes

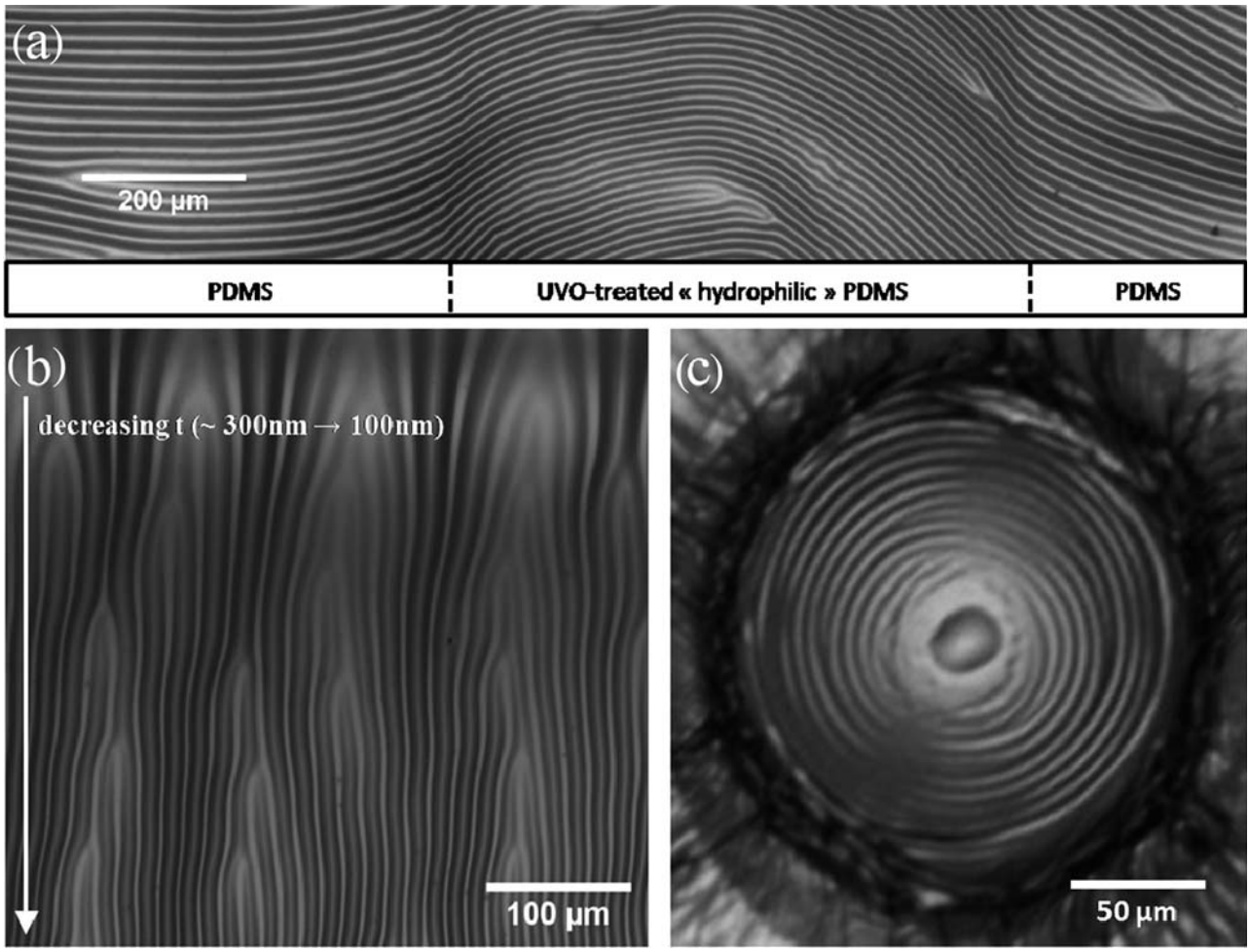

Fig. 4 Demonstration of the ability to dictate the shape of the wrinkles by controlling the three point contact line. (a) "Curly" wrinkles obtained using partially UVO-treated PDMS, creating zones with different wettability (hydrophobicity). (b) Creation of connected microchannels with different wavelengths using a gradient thickness film coated perpendicularly to the flow. Note the branching structures revealing strain localization. (c) Formation of circular wrinkles obtained by coating a PS film on a topographically modified triblock gel.

occurring at the contact line and can be explained with scaling arguments based on the mechanics of the contact line. Taking advantage of both the velocity and the directional dependence of adhesion on the three point contact line (and the ability to easily and finely tune these parameters), we are able to easily design unique patterns, on centimetric length scales, that can be of a great relevance for many applications. We speculate that because of the general existence of a contact line whenever two materials are brought into contact, these phenomena will also appear in countless contact geometries (*i.e.* cylinders in reel to reel processing) of direct practical interest to industry.

Experimental

Substrates

Crosslinked polydimethylsiloxane [PDMS] was prepared by mixing Dow Corning Sylgard 184 with catalyst and degassing for 30 min. The ratio catalyst/prepolymer was varied between 1 : 20 to 1 : 40. After verifying that the PDMS thickness does not play a role in the results obtained, the mixture was spun coated at 200 rpm on a glass slide for 2 minutes to ensure a homogeneous sample thickness (~250 μm) and prevents the PDMS from bending. The samples were then cured for 2 h in a 70 °C oven. The moduli of the substrates were measured using a contact mechanics setup recording force *vs.* displacement of a 1mm radius cylindrical silica probe ($E_{\mathrm{PDMS\ 1:20}} = 750 \pm 80$ kPa, $E_{\mathrm{PDMS\ 1:30}} = 400 \pm 50$ kPa, $E_{\mathrm{PDMS\ 1:40}} = 120 \pm 20$ kPa).

Complementary experiments were performed using a well characterized triblock gel: poly(methyl methacrylate)-*co*-poly(*n*-butyl acrylate)-*co*-poly(methyl methacrylate) (PMMA–PnBA–PMMA) (Kuraray Co, Ltd.) triblock gel solutions consisting of 15 wt% polymer (25k–116k–25k) in 2-ethyl-1-hexanol were heated to 85 °C as described in ref. 33 and 34 and molded in rectangular samples (25 mm × 30 mm × 1 mm). The molds were then removed from heat, covered, and allowed to adjust to room temperature, and the triblock gel substrates were used immediately after. The modulus of the gel substrates was measured using the same setup with a spherical silica indenter ($R = 5$ mm) and a JKR type analysis. The measured modulus of the gel was 4.5 kPa.

Films

Two different polystyrene [PS] molecules were purchased from Polymer Source Inc. (M_n = 876 kg mol^{-1}, I_p = 1.19 and M_n = 1.1 Mg mol^{-1}, I_p = 1.19). PS solutions in toluene were prepared at several concentrations (1, 2 and 3 wt%) and subsequently spun coat on a glass slide at several speeds varied from 1000 rpm to 6000 rpm. The samples with the lower molecular weight were then annealed 2 h in a 120 °C oven whereas the others were used as prepared. The film thicknesses were measured using AFM (Veeco Dimension 3100) and thicknesses from 50 nm to 600 nm were studied.

Gradient films were prepared using a custom-built programmable flow-coater.[35]

Wrinkling experiment

The substrate slide was fixed on an automated stage (Newport) allowing the control of the angle with a 0.1° precision and the pulling speed in the 0.01–5 mm s^{-1} range using a Labview interface, with additional experiments performed by evaporation (roughly 5 × 10^{-5} mm s^{-1}). The substrate was then partly immersed in a container of deionized water. A PS film was subsequently floated on the water and attached to the substrate at the water contact line. The substrate is then pushed in (or pulled out of) the water at a constant chosen speed (see Fig. 1), allowing the PS to slowly attach to the elastomer or gel. As the substrate is removed from the water bath, well aligned sinusoidal wrinkles following the contact line form over large length scales. The wavelength of the wrinkles was measured by AFM (Veeco Dimension 3100), optical profilometry (Zygo NewView 7300, 50× objective) and optical microscopy (Zeiss AxioTech Vario, 5× or 10× objective, Pixel Link CCD camera) with ImageJ to perform Fourier analysis on the images. The average wavelength was determined by collecting data from at least 4 locations on each sample. The amplitude of the wrinkles was measured by AFM and optical profilometry. The lower molecular weight PS was used with elastomeric samples, and the higher molecular weight PS was used with the triblock samples. Experiments performed at various angles (20–70°) showed no significant impact on the results obtained (data not shown): in consequence, the angle has been fixed at 45° in the experiments presented in the manuscript.

Acknowledgements

Funding for this work was provided by the Polymer-Based Materials for Harvesting Solar Energy—Energy Frontier Research Center funded by the US Department of Energy, Office of Science, Office of Basic Energy, Sciences under Award Number DE-SC0001087, as well as DARPA, and the NSF MRSEC (NSF DMR-0820506). The authors would like to thank Ms K. Best and Mr H. S. Kim for the preparation of the gradient films, and Dr D. Shandra for carefully reading the manuscript. ABC would like to thank J. Eggers for stimulating discussion regarding the fluid dynamics at the contact line.

Notes and references

1 S. P. Timoshenko and S. Woinowsky-Krieger, in *Theory of Plates and Shells*, McGraw-Hill, Singapore, 1959.
2 J. Genzer and J. Groenewold, *Soft Matter*, 2006, **2**, 310.
3 N. Bowden, S. Brittain, A. G. Evans, J. W. Hutchinson and G. M. Whitesides, *Nature*, 1998, **393**, 146.
4 E. Cerda and L. Mahadevan, *Phys. Rev. Lett.*, 2003, **90**, 074302.
5 C. M. Stafford, C. Harrison, K. L. Beers, A. Karim, E. J. Amis, M. R. Vanandingham, H. C. Kim, W. Volksen, R. D. Miller and E. E. Simonyi, *Nat. Mater.*, 2004, **3**, 545.
6 J. J. Groenewold, *Physica A (Amsterdam)*, 2001, **298**, 32.
7 H. Q. Jiang, D. Y. Khang, J. Z. Song, Y. G. Sun, Y. G. Huang and J. Rogers, *Proc. Natl. Acad. Sci. U. S. A.*, 2007, **104**, 15607.
8 H. Vandeparre and P. Damman, *Phys. Rev. Lett.*, 2008, **101**, 124301.
9 X. Chen and J. W. Hutchinson, *J. Appl. Mech.*, 2004, **71**, 597–603.
10 K. Efimenko, M. Rackaitis, E. Manias, A. Vaziri, L. Mahadevan and J. Genzer, *Nat. Mater.*, 2005, **4**, 293.
11 M. Ibn-Elhaj and M. Schadt, *Nature*, 2001, **410**, 796.
12 E. P. Chan and A. J. Crosby, *Adv. Mater.*, 2006, **18**, 3238.
13 A. K. Geim, S. V. Dubonos, I. V. Grigorieva, K. S. Novoselov, A. A. Zhukov and S. Y. Shapoval, *Nat. Mater.*, 2003, **2**, 461.
14 E. P. Chan, E. J. Smith, R. C. Hayward and A. J. Crosby, *Adv. Mater.*, 2008, **20**, 711.
15 Y. Xia and G. M. Whitesides, *Angew. Chem., Int. Ed.*, 1998, **37**, 550.
16 G. M. Whitesides, *Nature*, 2006, **442**, 368.
17 T. Ohzono, H. Monobe, K. Shiokawa, M. Fujiwara and Y. Shimizu, *Soft Matter*, 2009, **5**, 4658.
18 Y. Ito, *Biomaterials*, 1999, **20**, 2333.
19 D. Long, A. Ajdari and L. Leibler, *Langmuir*, 1996, **12**, 1221.
20 R. Pericet-Camara, G. K. Auernhammer, K. Koynov, S. Lorenzoni, R. Raiteri and E. Bonaccurso, *Soft Matter*, 2009, **5**, 3611.
21 *Polymer Data Handbook*, ed. J. E. Mark, Oxford University Press, New York, 1999, p. 833.
22 K. L. Johnson, *Contact Mechanics*, Cambridge University Press, Cambridge, 1987, p. 15.
23 R. Pericet-Camara, A. Best, H.-J. Butt and E. Bonaccurso, *Langmuir*, 2008, **24**, 10565.
24 K. R. Shull, *Mater. Sci. Eng., R*, 2002, **36**, 1.
25 J. Eggers, *Phys. Fluids*, 2005, **17**, 082106.
26 P. G. G. de Gennes, *Colloid Polym. Sci.*, 1986, **264**, 463.
27 T. D. Blake, *J. Colloid Interface Sci.*, 2006, **299**, 1.
28 L. Pocivavsek, R. Dellsy, A. Kern, S. Johnson, B. Lin, K.-Y. C. Lee and E. Cerda, *Science*, 2008, **320**, 912.
29 J. Yin and X. Chen, *Philos. Mag. Lett.*, 2010, **90**, 423.
30 D. Breid and A. Crosby, *Soft Matter*, 2009, **5**, 425–431.
31 G. Cao, X. Chen, C. Li, A. Ji and Z. Cao, *Phys. Rev. Lett.*, 2008, **100**, 036102.
32 N. Tsapis, E. R. Dufresne, S. S. Sinha, C. S. Riera, J. W. Hutchinson, L. Mahadevan and D. A. Weitz, *Phys. Rev. Lett.*, 2005, **94**, 018302.
33 P. L. Drzal and K. R. Shull, *Macromolecules*, 2003, **36**, 2000.
34 M. E. Seitz, W. R. Burghardt, K. T. Faber and K. R. Shull, *Macromolecules*, 2007, **40**, 1218.
35 J. C. Meredith, A. P. Smith, A. Karim and E. J. Amis, *Macromolecules*, 2000, **33**, 9747.

